BMC Genomics

RESEARCH

Open Access

Profiling the polyadenylated transcriptome of extracellular vesicles with long-read nanopore sequencing

Juan-Carlos A. Padilla[1,2], Seda Barutcu[1], Ludovic Malet[1], Gabrielle Deschamps-Francoeur[1], Virginie Calderon[1], Eunjeong Kwon[1] and Eric Lécuyer[1,2,3*]

Abstract

Background While numerous studies have described the transcriptomes of extracellular vesicles (EVs) in different cellular contexts, these efforts have typically relied on sequencing methods requiring RNA fragmentation, which limits interpretations on the integrity and isoform diversity of EV-targeted RNA populations. It has been assumed that mRNA signatures in EVs are likely to be fragmentation products of the cellular mRNA material, and the extent to which full-length mRNAs are present within EVs remains to be clarified.

Results Using long-read nanopore RNA sequencing, we sought to characterize the full-length polyadenylated (poly-A) transcriptome of EVs released by human chronic myelogenous leukemia K562 cells. We detected 443 and 280 RNAs that were respectively enriched or depleted in EVs. EV-enriched poly-A transcripts consist of a variety of biotypes, including mRNAs, long non-coding RNAs, and pseudogenes. Our analysis revealed that 10.58% of all EV reads, and 18.67% of all cellular (WC) reads, corresponded to known full-length transcripts, with mRNAs representing the largest biotype for each group (EV = 58.13%, WC = 43.93%). We also observed that for many well-represented coding and non-coding genes, diverse full-length transcript isoforms were present in EV specimens, and these isoforms were reflective-of but often in different ratio compared to cellular samples.

Conclusion This work provides novel insights into the compositional diversity of poly-A transcript isoforms enriched within EVs, while also underscoring the potential usefulness of nanopore sequencing to interrogate secreted RNA transcriptomes.

Keywords Extracellular vesicles, Long-Read RNA Sequencing, Nanopore sequencing, Polyadenylated transcriptome, Poly-A, mRNA, lncRNA, Transcriptomics, Transcript Isoforms, RNA-seq

Background

Extracellular vesicles (EVs) are a heterogeneous group of membrane-delimited nanoparticles of cellular origin [1, 2], which can act as protective vehicles for the extracellular trafficking and delivery of bioactive cargoes, including a diverse array of protein, DNA, and RNA molecules [2–6]. The transcriptome contained in EVs is reflective-of, but distinctive from the cells of origin, and is typically comprised of transcripts belonging to diverse RNA biotypes, including mRNAs and various classes of non-coding transcripts [7–10]. Upon

*Correspondence:
Eric Lécuyer
eric.lecuyer@ircm.qc.ca
[1] Institut de Recherches Cliniques de Montréal (IRCM), 110 Avenue des Pins, Ouest, Montréal, QC H2W 1R7, Canada
[2] Division of Experimental Medicine, McGill University, Montréal, QC H4A 3J1, Canada
[3] Département de Biochimie et de Médecine Moléculaire, Université de Montréal, Montréal, QC H3T 1J4, Canada

internalization or fusion with recipient cells, EVs can release these transcripts and, consequently, induce specific biological responses in recipient cells [11–15]. Indeed, the implications are wide ranging, from the promotion of tumorigenesis [16–18], to increased drug resistance in cancer [19–21]. As such, characterizing the RNA repertoire of EVs is an important element to understanding their biological properties.

The biological functions of RNAs are intrinsically tied to their sequence and structural features [22, 23]. For instance, the alternative splicing of pre-mRNAs allows the production of different mature mRNA isoforms from a single gene, substantially enhancing proteome complexity [24–26]. Moreover, different RNA isoforms may contain specific regulatory elements that modulate their functional properties in a variety of post-transcriptional regulatory processes, including RNA maturation [27], translation [28–30], stability [31], and subcellular localization [32]. As such, RNA sequence features are likely to be important determinants of secretion and of their activity in recipient cells following EV-mediated transfer. Strikingly, multiple reports of EV transcriptomes have indicated that various classes of coding and non-coding RNAs appear as fragments within EVs [8, 33–35], with some exhibiting biological relevance [35–38]. Even so, several studies have pointed to the transfer of functional mRNAs in recipient cells [7, 39–42].

Recently, long-read nanopore sequencing has emerged as a powerful technology for long-read RNA profiling, allowing the detection of full-length transcripts and unambiguous mapping of isoform diversity, thereby offering a great advantage over traditional sequencing methods that require fragmentation of the starting RNA material [43–46]. Using nanopore sequencing, we sought to compare the full-length poly-A transcriptome signatures of human K562 cells and EVs, in order to better understand the integrity and sequence features of EV transcripts. Strikingly, we show that EVs contain a high proportion of full-length mRNAs and non-coding RNAs, and further show that these transcripts can exhibit differential isoform diversity ratios in EVs versus their cells of origin. Thus, long-read RNA sequencing approaches offer an attractive avenue to ascertain the sequence features of EV transcriptomes and to better predict their functional properties.

Results

Nanopore RNA sequencing identifies a variety of RNAs in cells and EVs

To investigate the sequence features of an EV-targeted transcriptome, we herein sought to apply nanopore long-read sequencing to RNA purified from whole cells (WC) or EVs of the human chronic myelogenous leukemia cell line K562. For this, we employed a poly-A priming approach utilizing a PCR-cDNA barcoding strategy, which enables one to sequence full-length transcripts generated through reverse-transcription of poly-A + material (Fig. 1A). EVs were purified from K562 cell conditioned media (CCM) through centrifugation-based filtering and size exclusion chromatography (SEC) using qEVsingle 70 nm columns. Nanoparticle tracking analysis (NTA) was performed on purified EV material, which detected the presence of nanoparticles ranging from 100–600 nm in diameter (Fig. 1B). Furthermore, transmission electron micrographs (TEM) of the recovered material identified circular structures displaying the biconcave morphologies typically associated with EVs (Fig. 1C). RNA isolated from EV and cellular samples was subjected to Bioanalyzer automated electrophoresis to assess the concentration and quality of the preparations, revealing standard RNA integrity values typical of such specimens (Figure S1A). However, EV RNA displayed less pronounced peaks for 18S and 28S ribosomal RNA than was observed in cellular RNA (Figure S1A). Similar analysis of PCR-cDNA sequencing libraries showed that EV cDNA specimens display a biphasic size distribution, with a broader population > 700 nt similar to cellular samples, as well as a weaker population in the ~ 150–200 nt size range (Figure S1B). For sequencing, WC and EV libraries from the same replicate specimen were combined in the same nanopore flow cell at a ratio of 2:1. Consistent with this loading scheme, we obtained averages of 66.3% and 31.4% barcoded reads representing WC and EV, respectively (Figure S1C). Initial analysis of sequencing data demonstrated an average of ~ 8M reads per sequencing run, with an average of 62% of the raw reads passing the minimum quality score during base-calling (Figure S1D).

Among the reads that passed quality control, a higher proportion of mappable reads were obtained for WC (~ 88%) comparted to EV (~ 56%) specimens, with unmappable reads presenting characteristics of repetitive sequences (Figure S1E). Further interrogation of mappable reads revealed a similar proportion (~ 65%) of assigned versus unassigned (UA) reads across all samples (Fig. 1D), with ~ 15% of UA reads respectively being classified as either ambiguous (i.e., deriving from regions overlapping multiple genes) or NoFeatures (i.e., mapping to a region of the genome that does not contain any known gene). Principal component analysis (PCA) was performed on the sequencing libraries, revealing good segmentation of cellular and EV replicates into two clusters (Figure S1F). To evaluate the overall diversity of RNAs present in the sequencing data, their biotype assignations were assessed in transcripts per million (TPM). The groupings included 3 major classes: mRNA, lncRNA, and all RNA with a 'pseudogene'

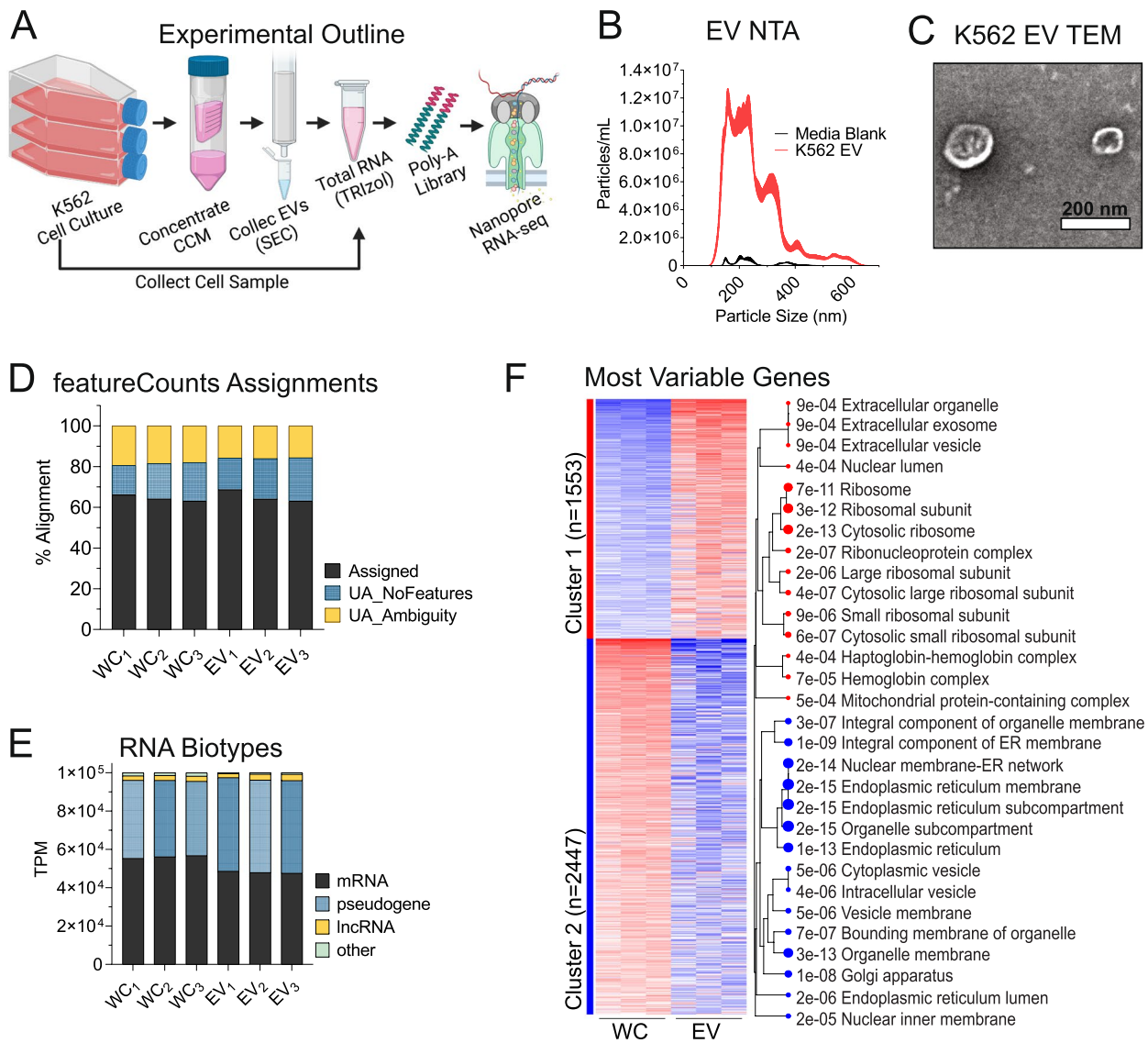

Fig. 1 Nanopore sequencing identifies a variety of RNA biotypes. **A** Graphical experimental outline of the isolation of K562 cellular and extracellular vesicles (EV) total RNA, library preparation, and nanopore sequencing. Graphic created with BioRender.com **B** Nanoparticle Tracking Analysis (NTA) of cleared cell-conditioned media. Border thickness defines the standard error. **C** Transmission electron micrographs of iodixanol gradient-purified EVs. EVs were negatively stained with 2% uranyl acetate and imaged on the FEI Tecnai T12 120kV transmission electron microscope. **D** Stacked bar graphs of the percentage of input of cellular and EV sequencing reads with assigned or unassigned (UA) features as determined by featureCounts. **E** RNA biotype distributions of cellular and EV transcriptomes. 'Other' includes a varied group of minor transcripts including, but not limited to, miscRNA, snRNA, snoRNA, etc. **F** iDEP unsupervised clustering heatmap of the top 4000 most variable genes in cellular and EV transcriptomes. Cellular component gene ontology (GO) terms associated with each cluster are represented on the right. Red lines denote enrichment in EVs, blue lines denote enrichment in cells

designation, while all minor classes of RNAs (e.g., miRNA, snoRNA, snRNA, miscRNA) were grouped as 'other' and accounted for < 1% of all assigned reads. These results showed that, in both cells and EVs, most transcripts detected were mRNAs or pseudogene transcripts, with a smaller number representing lncRNAs (2–3%). While EVs had similar proportions of mRNAs to pseudogene-derived transcripts (~ 48% each), cellular samples contained a higher proportion of mRNA (~ 56%) versus pseudogene (~ 40%) transcripts (Fig. 1E). Next, DESeq2 normalized counts were subject to iDEP differential expression and pathway analysis. A k-Means clustered heatmap was assembled of the top 4000 most variably expressed coding genes, and their associated

gene ontology (GO) enrichments for cellular components (CC) was determined. Unsupervised clustering revealed that EV mRNAs were enriched for functional classes associated with extracellular vesicles, ribosomal subunits, and ribonucleoprotein complexes, while WC-enriched mRNAs had functional signatures associated with diverse intracellular compartments (Fig. 1F).

Long-read RNA sequencing reveals EV-enriched and -depleted transcripts

A deeper analysis of differentially expressed transcripts between WC and EV samples revealed a total of 280 and 443 transcripts that were respectively enriched within WC or EV samples, while 10,865 RNA were similarly detected in both specimen types (Fig. 2A-B). EV-enriched RNAs included various RNA biotypes, with lncRNA (42.9%), pseudogenes (35.5%), and mRNA (13.7%) representing the major classes [%TPM]. In WC specimens, enriched RNAs included mostly lncRNA (78.6%), with pseudogenes (15.6%) and mRNA (5.6%) representing smaller populations [%TPM] (Fig. 2B). Although transcriptomic signatures across various biotypes were recorded for both cellular and EV specimens, the EV groups were the only class that demonstrated enrichment for other biotype classes, including snRNA, 5S rRNA, and Y-RNA. Interestingly, the sequencing reads associated to these RNAs contained varied lengths of poly-A at their 3' end (data not shown).

The top EV-enriched RNAs included 107 mRNA, 14 lncRNA, 287 pseudogenes, and 35 assorted non-coding RNA (Fig. 2B). The top 10 EV-enriched mRNA and lncRNA are represented in Fig. 2C-D. By contrast, the top cell-enriched RNAs included 198 mRNA, 47 lncRNA, and 35 pseudogenes (Fig. 2B). The top 10 cell-enriched mRNA and lncRNA are represented in Fig. 2E-F. Interestingly, cell-enriched mRNA encode for various members of the Speedy/RINGO family of proteins, which have been associated with mammalian cell cycle regulation through the activation of Cyclin-dependent kinases [47]. To determine whether the EV- or WC-enriched transcripts were associated to known gene ontology molecular functions, they were subjected to over-representation analyses (ORA) with g:Profiler. Our results showed that these EV-enriched transcripts were associated to various molecular functions relating to RNA metabolism, including structural constituents of the ribosome, pre-mRNA splicing, and RNA binding proteins (Fig. 2G, Figure S2A-B). Contrastingly, cell-enriched mRNAs associated to varied gene ontology terms relating to molecular function, including kinase binding, enzyme binding, and protein binding (Fig. 2H, Figure S2A-B).

EVs contain full-length RNAs and display preferential isoform recruitment

We next sought to interrogate our nanopore sequencing data to evaluate the presence of full-length RNA molecules across different biotypes relative to transcript isoforms that could represent shorter transcription or degradation products. To clarify these questions, we used BamSlam, a tool developed to analyse sequence length statistics of nanopore long-read sequencing data [48]. Mapping to the GENCODE v41 human transcriptome, sequenced transcripts displayed a median primary alignment > 91% for both cell and EV libraries (Fig. 3A). Following the recommendations made by BamSlam's authors, we considered transcripts as "full-length" if they covered > 95% of their annotated transcript. Applying these criteria revealed that 10.58% of all identified EV transcripts were full-length, whereas 18.67% of cellular RNAs were full-length (Fig. 3B). While cellular samples displayed a greater diversity, relative to EV samples, in the size distribution of their full-length transcripts (Fig. 3C-D), the mean coverage fraction in relation to the transcripts' lengths displayed similar profiles across both WC and EV transcriptomes (Fig. 3C-D). Interestingly, although the median alignment length of EV transcripts was shorter than those of cells (459 nt to 618 nt, respectively), the median length of all unique EV transcripts identified was 2,050 nt, while their cellular counterparts were 1,683 nt (Fig. 3E). These findings were reflective of the GENCODE v41-mapped reads, which displayed similar median alignment lengths and size distribution profiles to those identified by BamSlam (Figure S3A-C). Curiously, unmapped reads (excluded from BamSlam analyses) were generally under 150 nt in length in both WC and EV specimens (Figure S3D-E).

(See figure on next page.)

Fig. 2 EV-enriched RNAs display GO associations to ribonucleoprotein complexes. **A** Volcano plot of cellular and EV transcriptomes signifying the shift in gene expression levels. Blue dots represent statistically significant downregulated EV-genes (Log_2 fold change ≤ -2, *P*adj ≤ 0.01). Red dots represent statistically significant upregulated EV-genes (Log_2 fold change ≥ 2, *P*adj ≤ 0.01). **B** Venn diagram of differentially expressed RNAs in EV vs WC (Log_2 fold change ≥ 2 or ≤ -2, *P*adj ≤ 0.01). In the center are RNAs which displayed similar expression profiles in either group. Inclusion to this group was limited to RNAs with an average of ≥ 5 reads (triplicates). Differentially expressed RNAs are further categorized into pie charts and bar graphs, denoting their relative percentages in transcripts per million and their contributing RNAs, respectively. **C-D** Bar graphs of the top 10 EV-enriched (Log_2 fold change ≥ 2, *P*adj ≤ 0.01) mRNA and lncRNA, respectively. **E–F** Bar graphs of the top 10 cell-enriched/EV-depleted (Log_2 fold change ≤ -2, *P*adj ≤ 0.01) mRNA and lncRNA, respectively. **G** Bubble plot of GO molecular function of EV-enriched mRNA as determined with g:Profiler. All enriched (Log_2 fold change ≥ 2, *P*adj ≤ 0.01) RNA considered. **H** Bubble plot of GO molecular function of cell-enriched mRNA as determined with g:Profiler. All enriched (Log_2 fold change ≤ -2, *P*adj ≤ 0.01) RNA considered

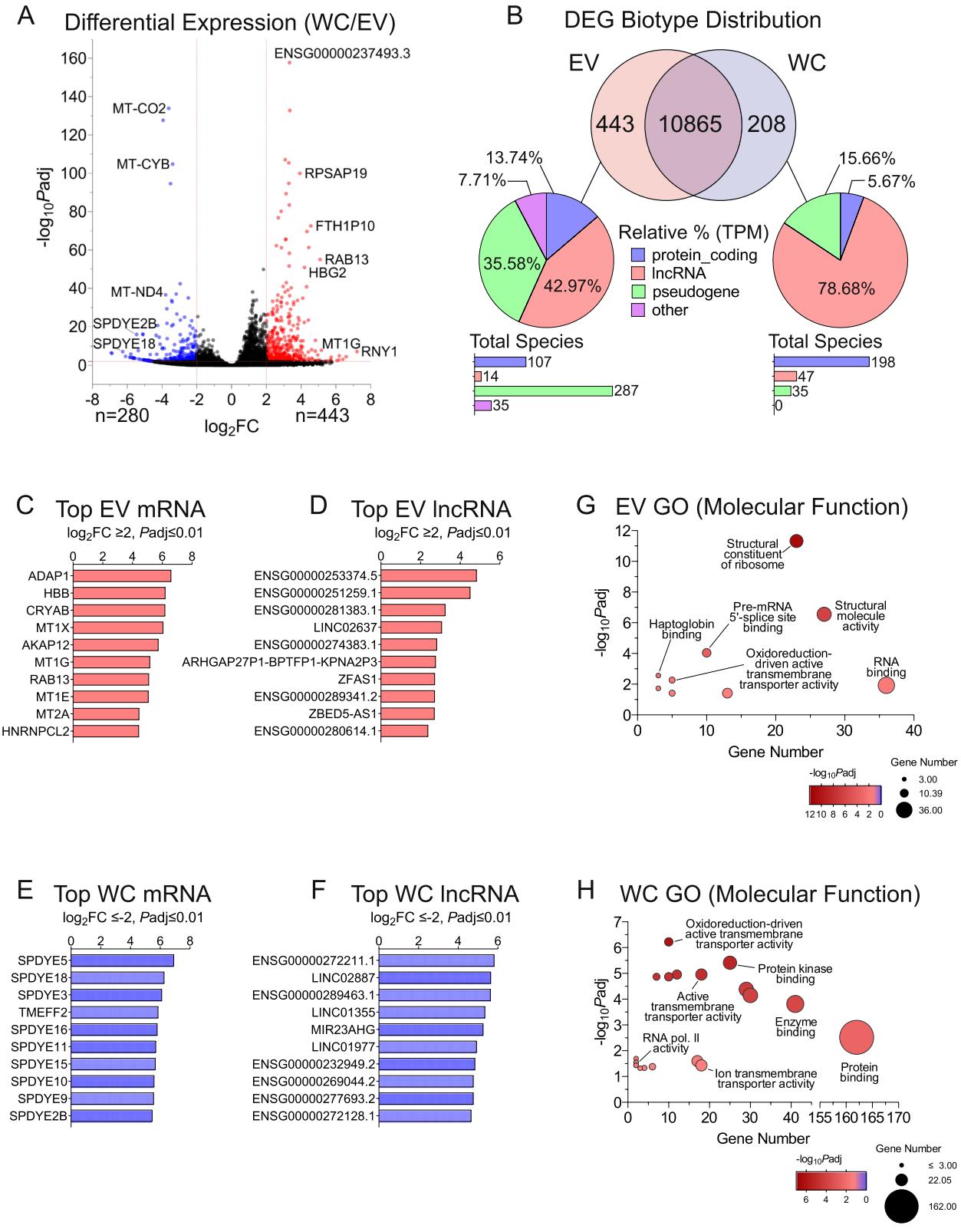

Fig. 2 (See legend on previous page.)

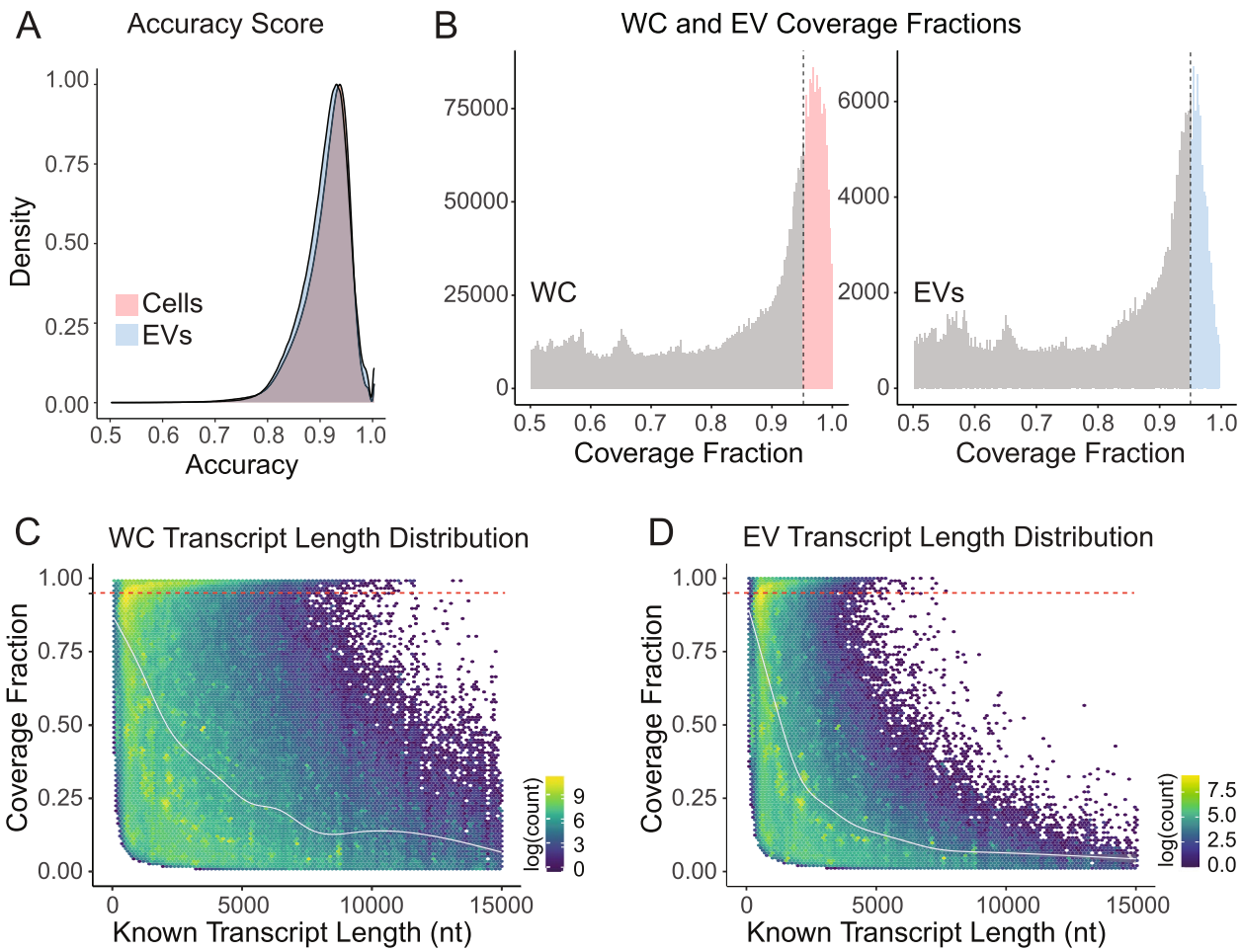

E Summary of Full-Length Coverage Statistics

Sample	WC Reads	EV Reads
Total number of reads	6887456	1410601
Full-length transcripts	1285568	149243
% full-length transcripts (of total)	18.67	10.58
Median alignment length (primary alignments)	618	459
Median coverage fraction (primary alignments)	0.57	0.45
Median accuracy (primary alignments)	91.86	91.54
Reads with no secondary alignments	1384348	188554
% reads with no secondary alignments	20.10	13.37
Unique transcripts identified	110919	53975
Median coverage fraction (unique transcripts)	0.34	0.22
Median length (unique transcripts)	1683	2050

Fig. 3 EVs contain full-length RNAs. **A** Median accuracy of primary alignment score determined using the BamSlam algorithm. **B** Histogram distribution of full-length reads in cells and EVs. Represented are the coverage fractions of known transcript length covered by each read (truncated at 0.5). The dotted lines represent the > 95% coverage denoting full-length. Full-length cellular transcripts shown in red, full-length EV transcripts shown in blue. **C**-**D** Density plots of cellular (**C**) and EV (**D**) transcripts displaying their coverage fractions against known transcripts. **E** Summary of statistical information as determined by BamSlam

Next, we assessed whether full-length read coverages displayed RNA biotype specific differences. As shown in Fig. 4A, comparison of transcript coverage fractions across different RNA biotypes revealed a general similarity in coverage scores between WC and EV specimens. Strikingly, for several biotypes, including mRNAs, lncRNAs and pseudogene-derived transcripts, we observed prominent enrichment for short isoforms, both within WC and EV sequencing datasets. By contrast, RNA families made up of shorter RNA molecules, such as snRNAs, snoRNAs and miscRNAs, had a larger proportion of transcripts displaying greater isoform coverages. Focusing our analyses on full-length RNAs, across all RNA biotypes, revealed that the diversity of full-length transcripts is markedly different between WC and EV specimens, with cells having a larger proportion of full-length pseudogenes (10.3%), while EVs had a higher proportion of full-length mRNA transcripts (58.1%) (Fig. 4B-C). These findings differ from the overall BamSlam-identified population of genes (Fig. 4D-E), which showed the presence of large proportions of reads corresponding to mRNAs in cells and to classes such as lncRNAs and "other" RNAs in EVs, but whose values were reduced in the full-length transcript populations, suggesting fragmented products.

Finally, we investigated whether EV specimens display differential recruitment of transcript isoforms relative to their cells of origin. Using the Full-Length Alternative Isoform Analysis of RNA (FLAIR) tool [49], we conducted differential splicing and isoform analyses of the WC and EV transcriptomes. Remarkably, the identified RNAs included transcript isoforms that were under- or over-represented in EV or WC specimens, demonstrating the occurrence of transcript isoform-specific recruitments in the EV population (Figure S4A-B). Our results show that, depending on the gene, WC and EV transcript populations can exhibit different levels of similarity. In some cases, the isoform distributions were very similarly between WC and EV specimens, as exemplified by the case of *RPL10* mRNA isoforms (Fig. 5A). By contrast, analysis of mRNA isoforms derived from the *ELOVL5* and *HSPA9* genes revealed a striking shift in isoform representation in EV versus cellular specimens (Fig. 5B-C). We further compared the read intensities of these representative RNAs to Illumina short-read sequencing data from K562 EVs (unpublished data) (Fig. 5A-C). These results show that while read coverage is similar in both instances, long-read nanopore sequencing data exhibits more homogeneity across read regions. Interestingly, further analysis of EV-enriched isoforms revealed that they were not truncated in both EV and WC samples (Figure S4C). Conversely, WC-enriched isoforms exhibited adequate coverage in WC samples but lacked coverage in EV samples, indicating that they may either be absent in the EV samples or truncated (Figure S4C). In addition, we analysed the length distributions of EV or WC-enriched transcripts. Our findings indicate that although the lengths of genes containing differentially expressed isoforms are not smaller in EVs compared to cells (Figure S4D), the lengths of the isoforms themselves are reduced in EVs (Figure S4E). Altogether, these results demonstrate that EVs can carry a diversity of full-length RNAs, displaying enrichments for a subset of these, and can further incorporate preferred isoforms relative to their cells of origin.

Discussion

Extracellular vesicles have gained prominence as novel mediators of the exchange of information between cells [50, 51]. This ability is bestowed by their loading with bioactive molecules, including RNAs, which can influence the behaviour of recipient cells [52–55]. The profiling of EV transcriptomes has contributed significantly to the identification of disease-associated biomarkers [56–60] and, furthermore, has linked numerous EV RNAs to the progression of disease [40, 61–64]. Here we report on the full-length transcriptomes of human K562 cells and EVs, as determined by long-read nanopore sequencing. Using size exclusion chromatography (SEC) with commercially validated columns, we isolated a broad population of EVs, which were confirmed with transmission electron micrographs. This allowed us to demonstrate that nanopore sequencing can be used to identify the diverse RNA biotypes and isoforms present within EVs, with sufficient sensitivity to determine their differential expression (Figs. 1 E–F and 2A-F). Interestingly, these transcripts can include a diversity of sequence lengths, with many appearing as full-length RNAs (Fig. 3C-E) that exist in WC- or EV-specific biotype proportions (Fig. 4B-C). Strikingly, we show that EV-trafficked RNAs can also exhibit isoform-specific recruitments, with certain isoform variants being more abundant in the EV transcriptome (Fig. 5A-B).

While the transcripts that can be identified in EVs generally represent the RNAs found in parental cells, there is a marked specificity in the recruitment of particular RNA species to the EV population [9, 10, 65]. Indeed, long-read nanopore sequencing of WC and EV RNA demonstrated specimen-specific differential expressions for diverse RNAs, with 443 EV-enriched and 280 cell-enriched transcripts detected (Fig. 2B). Interestingly, while these transcripts demonstrate GO-enrichments to extracellular vesicles and the extracellular space (Fig. 1F, Figure S2A), they were also highly associated to various ribonucleoprotein complexes and included structural components of the ribosome and the U1 spliceosome (Fig. 2G, Figure S2A-B). Various coding, non-coding, and

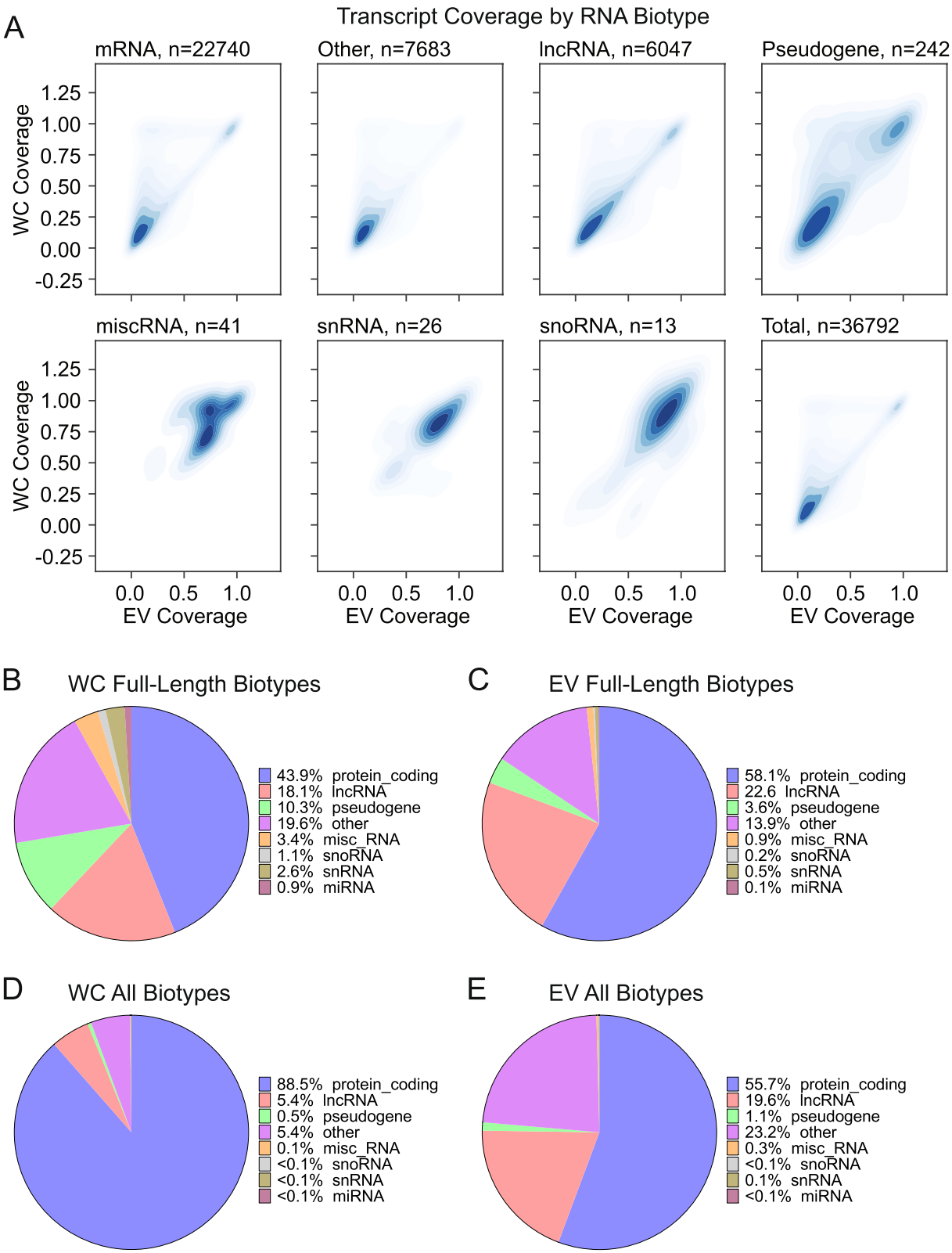

Fig. 4 EVs contain full-length RNAs of different biotypes. **A** Density plots of RNA biotypes displaying the transcript coverage in EVs relative to cells. **B-C** Pie charts displaying the RNA biotype percentages of BamSlam-identified full-length RNAs identified in cells and EVs. **D-E** Pie charts displaying the RNA biotype percentages of all BamSlam-identified RNAs (full-length and non-full-length) identified in cells and EVs

pseudogene RNAs were highly enriched in EVs (Fig. 2B-F). This is consistent with previous reports, including our own, that EVs are enrichment for various RNA biotypes such as Y-RNAs, mRNAs, spliceosomal RNAs, and pseudogenes transcripts [8, 10, 35, 42, 66–68]. The presence of these specific non-coding RNAs (ncRNAs) in EVs, despite their atypical enrichment through poly-A selection, was consistently observed across multiple replicates. Furthermore, their corresponding reads exhibited stretches of poly-A (Figure S2C). Nevertheless, the possibility of unspecific binding of the poly-dT primer during cDNA synthesis cannot be ruled out. It is worth mentioning, however, that the polyadenylation of ncRNAs is not uncommon, as it has been previously observed in eukaryotes, including human cells [69–73]. In contrast, the cellular transcriptome displayed an enrichment for various members of the Speedy/RINGO family of non-canonical Cyclin-dependent kinases (CDKs) (Fig. 2E). Proteins of this family have been associated with the activation of CDKs during cell cycle regulation and cell proliferation, moreover they may be overexpressed in various cancers [47, 74–76]. Although Speedy/RINGO mRNAs are detected in our K562 EV transcriptomes, their enrichment lies with the cellular specimens.

Various reports have pointed to populations of fragmented coding and non-coding transcripts present in EVs [8, 33–38], and the extent to which full-length transcripts may be incorporated into EVs remains unclear. Recently, Li et al. provided some insight into this pervasive question [56]. They developed the extracellular vesicle long RNA sequencing (exLR-seq) technique, whereby EV RNAs were used to generate sequencing libraries using the SMARTer® Stranded Total RNA-Seq Kit (Clontech) followed by the sequencing of 150 bp pair-end reads on the Illumina platform [56]. By utilizing bioinformatic tools, they demonstrated that numerous EV mRNAs exhibited similar coverage across both the UTRs and CDS regions, indicating full-length coverage [56]. These findings align with our previous observations [10]. The approach described herein provides more pointed evidence, as it employs the use of long-read sequencing technology to investigate EV RNAs without having to subject them to fragmentation steps. To investigate the proportion of full-length transcripts present in our sequencing data, we utilized the bioinformatic tool BamSlam [48], which enabled us to calculate sequence length statistics by mapping the sequencing reads to the human transcriptome (GRCh38.p13, transcript sequences [GENCODE v41]). This analysis revealed that 10.6% of all reads in EVs spanned across the reported full-length transcript to which they mapped (Fig. 3B,E). Strikingly, this proportion is only slightly lower than the population of full-length transcripts identified in their parental cells (Fig. 3D-E). Indeed, a surprising observation was that both WC and EV transcriptomes were comprised primarily of transcripts that were not classified as full-length (Fig. 3B-E). Nevertheless, WC transcripts were more diverse in their sequence lengths (Fig. 3C-D), with a ~ 150 nt difference between the median lengths of WC and EV transcripts (Fig. 3E). We further analysed our data to focus on the identification of transcript isoforms, and whether recruitment of isoforms is differential in the EV transcriptome. To this end, various possible approaches have been recently reported in the literature [49, 77, 78]. Using the Full-Length Alternative Isoform Analysis of RNA (FLAIR) tool [49], we show that while some EV RNAs may reflect the isoform diversity present in their parental cells (Fig. 5A), they may also carry preferred isoform variants (Figs. 5B-C, Figure S4A-B). This is quite revealing, as it suggests that the specificities in

(See figure on next page.)

Fig. 5 EVs carry differentially expressed transcript isoforms. **A** Isoform usage analysis of *RPL10* displaying recruitment of similar isoform types in EVs relative to cells of origin. The genome browser views represent the sequencing reads along with their associated transcript isoforms. LR represents long-read nanopore sequencing data, while SR represents Illumina short-read sequencing (unpublished data). Histograms represent the percentage of transcript isoform representation per transcriptome, with color coding matching the accompanying isoform. R = total number of detected reads. Isoform identity (as defined by FLAIR): Isoform 1: *6eee3e78-fe04-4ee6-90d4-ecc361ca6e05*, Isoform 2: *415620e2-1272-483b-86eb-7d7532fe4780*, Isoform 3: *ENST00000344746.8*, Isoform 4: *ENST00000436473.5*, Isoform 5: *ENST00000369817.7*, Isoform 6: *07d5ac1f-db7c-47ab-a5e8-04a78777867e*, Isoform 7: *40708139-1f87-49ca-a99a-5f5e1e0422c9*. **B** Isoform usage analysis of *ELOVL5* displaying preference for the recruitment of isoform variants in EVs relative to cells of origin, with variant *ENST00000370913.5* showing enrichment in EVs. The genome browser views represent the sequencing reads along with their associated transcript isoforms. LR represents long-read nanopore sequencing data, while SR represents Illumina short-read sequencing (unpublished data). R = total number of detected reads. Isoform identity (as defined by FLAIR): Isoform 1: *9d9223d4-0463-4bdf-ae2c-603abfbc8fae*, Isoform 2: *ENST00000542638.5*, Isoform 3: *a987f2f6-fdb0-4501-87c3-9b457392a133*, Isoform 4: *ENST00000304434.11*, Isoform 5: *ENST00000370913.5*, Isoform 6: *03f316c6-1d4c-48e5-ab63-57acbaaf3126*, Isoform 7: *4a5f7dbd-8838–4359-af96-63e1ff580847*. **C** Isoform usage analysis of *HSPA9* displaying preference for the recruitment of isoform variants in EVs relative to cells of origin, with variant *4671fbc1-2c63-4c88-af4b-90b6b1aa4277* showing enrichment in EVs. The genome browser views represent the sequencing reads along with their associated transcript isoforms. LR represents long-read nanopore sequencing data, while SR represents Illumina short-read sequencing (unpublished data). R = total number of detected reads. Isoform identity (as defined by FLAIR): Isoform 1: *ENST00000677988.1*, Isoform 2: *ENST00000678794.1*, Isoform 3: *ENST00000678384.1*, Isoform 4: *ENST00000678300.1*, Isoform 5: *ENST00000677553.1*, Isoform 6: *ENST00000297185.9*, Isoform 7: *4671fbc1-2c63-4c88-af4b-90b6b1aa4277*. For all figures, isoform shading corresponds to: solid color (productive), hatched color (premature termination codon), or faded color (no start codon or has start codon but no stop codon)

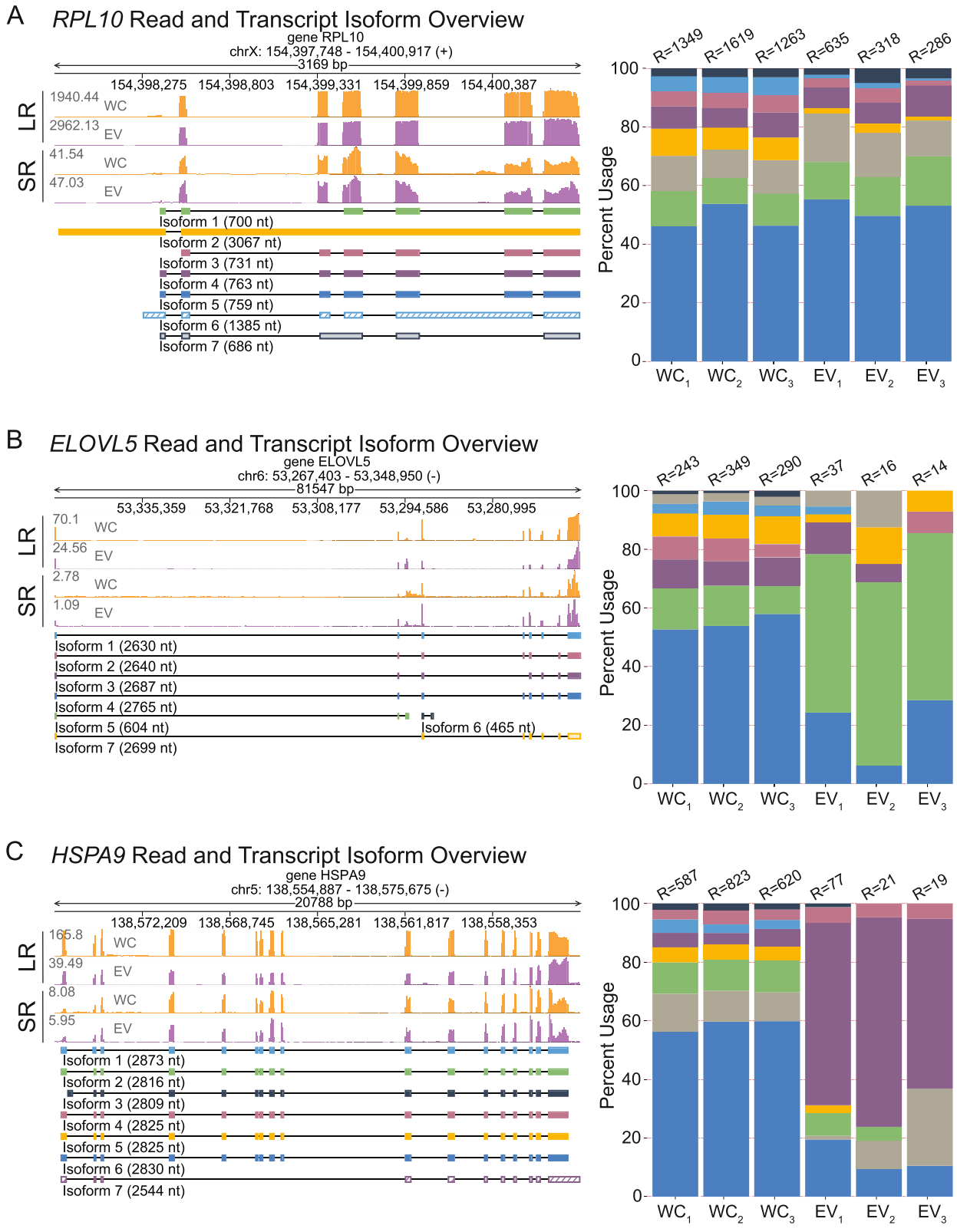

Fig. 5 (See legend on previous page.)

RNA recruitment during EV-biogenesis can extend to the transcript isoform level, while it remains to be determined if this selective packaging plays a significant role in the biological functions of EVs.

Conclusions

Here, we show that long-read nanopore RNA sequencing is a robust means for investigating the transcriptomes trafficked by extracellular vesicles, demonstrating that these data that can be used to explore the sequence features of extracellular RNA. Indeed, we provide compelling evidence demonstrating the existence of full-length polyadenylated RNAs within EVs derived from human cells. Furthermore, these RNAs can exhibit differential expression relative to their parental cells, with some displaying isoform-specific enrichments.

Currently, there is limited data on full-length poly-A transcripts in a broader range of extracellular vesicles (EVs) from different cell lines. Future studies using nanopore sequencing across multiple cell lines would be valuable for exploring and understanding the full-length poly-A transcripts carried by EVs. Importantly, we believe that the introduction of single-molecule long-read sequencing techniques, such as that described in this manuscript, will be instrumental in understanding the *cis*-regulatory elements driving RNA recruitment to sites of EV-biogenesis [6, 79–81], and furthermore, could be leveraged in the future to investigate the post-transcriptional modifications of EV transcriptomes [82–84]. Additionally, it would be interesting to combine these approaches with cellular fractionation techniques, such as CeFra-Seq [85, 86], to provide the additional spatial resolution needed to understand intracellular RNA trafficking pathways. In conclusion, our findings suggest that selective mechanisms modulate RNA isoform incorporation during EV biogenesis, adding additional complexity to our current understanding.

Methods

Cell culture conditions for EV collection

Human K562 Chronic Myelogenous Leukemia cells were routinely cultured in Roswell Park Memorial Institute (RPMI) 1640 medium with L-glutamate (Corning, 10–040-CV) supplemented with 10% foetal bovine serum (FBS), 100 U mL^{-1} penicillin and 100 µg mL^{-1} streptomycin (Wisent, 450–202-EL). The cells were grown under incubation conditions of 37 °C and humidified 5% CO_2 atmosphere. K562 cells were obtained as part of our collaboration with the Encyclopedia of DNA Elements (ENCODE) consortium (ENCBS036OIX).

For EV isolations, the same conditions were used, but the media contained 10% EV-depleted foetal bovine serum (dFBS), rather than 10% FBS. dFBS was prepared via tangential flow filtration (TFF) using the Labscale TFF System (Millipore-Sigma) equipped with a Pellicon XL50 ultrafiltration module with a 300 kDa Ultracell membrane (Millipore-Sigma, PXC300C50). K562 cells were plated starting at 1.75×10^7 cells per T-175 flask in 35 mL of media ($0.5x10^6$ cells/mL) in a total of 5 flasks per replicate ($n = 3$). The cells were incubated for 36 h at 37 °C in humidified 5% CO_2 atmosphere. After 36 h, the cell-conditioned media was collected, along with representative cellular samples. The cells were assessed for ≥ 95% cell viability by Trypan blue exclusion assay. The cell-conditioned media was used for purification of EVs.

EV purification approach

The purification of K562 EVs was conducted with size exclusion chromatography. The collected cell-conditioned media was pre-processed to clear it of cells and large debris by centrifugation at $500 \times g$ for 10 min, and $2000 \times g$ for 20 min, respectively. The cleared supernatant was collected and then concentrated by centrifugation at $2000 \times g$ with a 100 kDa NMWL Amicon Ultra-15 centrifugal filter unit (Millipore-Sigma, UFC910024) to a volume of 0.5 mL. The samples were collected and then concentrated further to 100 µL using 100 kDa NMWL Amicon Ultra-0.5 centrifugal filter unit (Millipore-Sigma, UFC510096). The final concentrated samples were recovered and used for the purification of EVs through size exclusion chromatography (SEC) with qEVsingle 70 nm columns (Izon Science, SP2-USD) following the manufacturer's recommendations. Briefly, 100 µL of concentrated media was loaded on the column and allowed to elute. Next, 900 µL of 0.1 µm-filtered phosphate-buffered saline (PBS) 1 × was loaded and allowed to elute, for a combined 1 mL void volume. Finally, 600 µL of 0.1 µm-filtered phosphate-buffered saline 1 × was loaded to the SEC column, and the eluted 600 µL was kept as the EV-enriched fraction. Purifications of EVs was conducted in biological triplicates.

Characterisations of purified EV samples

The eluted SEC samples ($n = 3$) were subjected to validation experiments to assess the presence and features of purified EVs. First, nanoparticle tracking analysis (NTA) was performed to verify the presence of nanoparticles of the size range in the EV preparations. NTA was conducted using a NanoSight NS500 system (Malvern Panalytical) equipped with the 532 nm laser, and by way of three 30 s recordings at 37 °C. Data processing and analysis was performed automatically by the NanoSight NTA software v3.0 (Malvern Panalytical). The data were exported and further analysed on Microsoft Excel (Microsoft Corporation) and visualized on GraphPad Prism (GraphPad Software Inc). Next, the samples were

subject to transmission electron microscopy (TEM) to corroborate the presence of EVs. Samples from the SEC-recovered eluates were combined 1:1 with a 5% glutaraldehyde solution (2.5% final concentration) for fixation. 5 µL of the fixed samples were then loaded to previously discharged formvar-coated copper grids and allowed to adhere for 3 min. The sample-containing grids were washed 3 times with water, and then placed in droplets of 2% uranyl acetate and incubated for 1 min. The grids were then washed 3 more times with water, blotted to remove excess water, and air dried for 30 mins. The grids were then imaged on the FEI Tecnai T12 120kV (Field Electron and Ion Company) transmission electron microscope. Sample preparation and imaging was carried out at the Facility for Electron Microscopy Research (FEMR) at McGill University.

RNA isolation

For each of the experimental replicates, representative K562 cells were collected and pelleted at 500×*g* for 5 min. The cellular pellets were resuspended in TRIzol reagent (Thermo Fisher, 15596018) to isolate RNA as per the manufacturer's recommendations. Briefly, the samples were homogenized in 500 µL of TRIzol reagent, after which 100 µL of chloroform was added (VWR, BDH1109-4LG). The samples were then centrifuged at 12,000×*g* for 15 min. Following the centrifugation, the aqueous phase was used for RNA purification using the RNA Clean & Concentrator-5 system (Zymo Research, R1013) with in-column DNase I treatment. All steps were performed according to the manufacturers' protocols. K562 EV samples were processed using TRIzol LS reagent (Thermo Fisher, 10296028), as it would prevent the need to pellet the samples and reduce loss of materials. For RNA purification, the SEC-eluted EV samples were homogenized in 1.8 mL of TRIzol LS reagent, after which 480 µL of chloroform was added (VWR, BDH1109-4LG). The samples were then centrifuged at 12,000×*g* for 15 min. The aqueous phase was processed for RNA purification as described above, using the RNA Clean & Concentrator-5 system with in-column DNase I treatment. All RNA samples were eluted in nuclease-free water and assessed for quality and concentration with Nanodrop and Bioanalyzer.

Preparation of RNA sequencing library

The purified cellular and EV RNA samples were utilized for preparation of sequencing libraries using the PCR-cDNA Barcoding Kit (Oxford Nanopore Technologies, SQK-PCB109), as per the manufacturer's guidelines, with some modifications. Briefly, cellular and EV samples were used for the preparation of cDNA starting with 50 ng of total RNA, followed by PCR amplification of each of the six libraries using a unique barcode per sample. The samples were subjected to 14 cycles of denaturation, annealing, and extension, and the products were purified using RNAClean XP beads (Beckman-Coulter, A66514), which can be used for both RNA and DNA purification. The purification of PCR products was conducted using the methods outlined by Oxford Nanopore. The bead-bound libraries were then eluted with 12 µL of Elution Buffer (EB) and quantified using the Qubit RNA Broad Range (BR) kit (Thermo Fisher, Q10211), as per the manufacturer's recommendations. The samples were further analysed with Bioanalyzer to assess the library quality.

Loading and sequencing of PCR-cDNA libraries

The sequencing of PCR-cDNA libraries was carried out using a MinION device (Oxford Nanopore Technologies, MIN-101B) equipped with a compatible Flow Cell R9.4.1 (Oxford Nanopore Technologies, FLO-MIN106D). Each loading library consisted of one cellular library and one EV library in a 2:1 ratio, respectively, and to a final loading concentration of ~ 100 fmol. This ratio was chosen as cellular sequencing libraries were expected to be comparatively more complex to EV sequencing libraries. Briefly, 66.66 fmol of cell library was combined with 33.33 fmol of EV library, and the volume was adjusted to 11 µL of Elution Buffer (EB). Next, 1 µL of Rapid Adapter (RAP) was added to the combined libraries, followed by a room temperature incubation of 5 min. The flow cell was then primed and loaded following the manufacturer's recommendations. Primary data acquisition was performed using the MinION Software (Oxford Nanopore Technologies, MinION Release 22.05.5) with default parameters, but no local basecalling. The sequencing of the loaded libraries was allowed to proceed for 72 h, after which the resulting FAST5 files were further processed bioinformatically.

Transcriptomics and bioinformatics analyses

To analyse the resulting FAST5 files, the nfcore/nanoseq pipeline was used as described previously [87]. Briefly, basecalling was performed on FAST5 files for each replicate with Guppy base caller software (Oxford Nanopore Technologies, v6.2.1) using a quality threshold of 7. Passing reads were then demultiplexed into individual barcodes using the FASTQ barcoding pipeline (demux_fast5) of the Oxford Nanopore Technologies Bioinformatics Platform. Reads shorter than 20 nucleotides were filtered out using NanoFilt [88]. Resulting FASTQ files were mapped to the human reference genome GENCODE v41 using minimap2 v2.24 with the option -ax splice [89]. Counts per million reads mapped (CPM)-normalized BedGraph files were generated from Binary Alignment/Map (BAM) files using the bamCoverage

tool from the deepTools suite [90]. BAM files were used as input to featureCounts from Rsubreads [91] for gene count and transcript quantifications in long-read mode using the GENCODE v41 annotation file. Next, differential expression analysis was performed with the DEseq2 R package [92] to identify significant EV-enriched or EV-depleted genes and transcripts. PCA was conducted using the gene counts obtained by featureCounts normalized by DESeq2.

The web-based integrated Differential Expression and Pathway analysis (iDEP) tool [93] was used to generate a k-Means heatmap of the normalized read count data. GraphPad Prism (GraphPad Software Inc.) was used to generate a volcano plot depicting the differentially expressed EV RNAs. Overrepresentation analyses (ORA) of gene ontology (GO) terms were executed on g:Profiler [94] (version e107_eg54_p17_bf42210) with the Benjamini–Hochberg false discovery rate multiple testing correction method and while applying significance threshold of 0.05. Gene lists included in these analyses were filtered for EV-enrichment [Log_2 fold change ≥ 2, *P*adj ≤ 0.01] or EV-depletion (i.e. cell-enriched) [Log_2 fold change ≤ -2, *P*adj ≤ 0.01]. Svist4get [95] was used to visualize genomic signal tracks of selected EV-enriched genes. Sequence length statistics were computed using the BamSlam script (https://github.com/josiegleeson/BamSlam) [48], requesting to re-run mapping steps with specific parameters for minimap2 with the options -ax map_ont –sam_hit_only. For representation purposes, BAM files were then sorted and indexed with SAMtools before merging by condition (cells and EV). Read coverage scores > 95% of the annotated transcript was considered as full-length. Differential splicing and isoform analyses were conducted by using the Full-Length Alternative Isoform Analysis of RNA (FLAIR) tool [49]. FLAIR modules *align*, *correct* and *collapse* were successively used for mapping FASTQ files to GENCODE v41, identifying splice junctions. Next, isoform quantifications were made with the *quantify* module, and the output count matrix was used to plot isoform structures and the percent usage of each isoform in each sample for a given gene. Finally, *predictProductivity* was utilized to predict isoform productivity with output definitions as PRO (productive), PTC (premature termination codon), NGO (no start codon), or NST (has start codon but no stop codon).

Abbreviations

× g	Relative centrifugal force
3′end	Three prime end
BAM	Binary Alignment/Map
BP	Biological process
CC	Cellular components
CCM	Cell-conditioned media
cDNA	Complimentary deoxyribonucleic acid
CO_2	Carbon dioxide
CPM	Counts per million reads mapped
DNA	Deoxyribonucleic acid
DNase I	Deoxyribonuclease I
EV(s)	Extracellular vesicles
FBS	Foetal bovine serum
fmol	Femtomole
GO	Gene ontology
kDa	Kilodalton
k-Means	Unsupervised method for clustering genes
lncRNA	Long non-coding ribonucleic acid
MF	Molecular function
miRNA	Microribonucleic acid
miscRNA	Miscellaneous ribonucleic acid
mRNA	Messenger ribonucleic acid
NMWL	Nominal molecular weight limit
NTA	Nanoparticle tracking analysis
ORA	Overrepresentation analysis
*P*adj	Adjusted P value
PCA	Principal component analysis
PCR	Polymerase chain reaction
Poly-A	Polyadenylated
Pre-mRNA	Precursor messenger ribonucleic acid
RNA	Ribonucleic acid
SEC	Size exclusion chromatography
snoRNA	Small nucleolar ribonucleic acid
snRNA	Small nuclear ribonucleic acid
TEM	Transmission electron microscopy
TFF	Tangential flow filtration
TPM	Transcripts per million
WC	Whole cell

Supplementary Information

The online version contains supplementary material available at https://doi.org/10.1186/s12864-023-09552-6.

Additional file 1: Figure S1. Library preparation and initial analyses. **Figure S2.** Gene ontology (GO) associations of EV and WC poly-A transcripts. **Figure S3.** Size distribution of EV-derived RNAs. **Figure S4.** Analyses of differentially expressed RNA isoforms.

Acknowledgements

The authors thank the Institut de Recherches Cliniques de Montréal (IRCM)'s Molecular Biology and Functional Genomics, and Bioinformatics platforms, as well as McGill University's Facility for Electron Microscopy Research for their support. In addition, we thank Janusz Rak and Laura Montermini for their support with NTA data acquisition.

Authors' contributions

J.C.A.P., S.B., and E.L. conceived the project and designed the experiments. J.C.A.P. isolated and characterized the EV samples, performed all RNA isolations and quality control steps, prepared sequencing libraries, and carried out the nanopore sequencing. J.C.A.P., S.B., L.M., G.D.F., E.K., and V.C. analysed the data. J.C.A.P. mounted the figures and wrote the manuscript. E.L., E.K., and S.B. provided critical feedback on the manuscript drafts. All authors read, edited, and approved the final manuscript.

Funding

This work was supported by grants to E.L. from the Canadian Institutes of Health Research (CIHR), the Natural Sciences and Engineering Research Council of Canada (NSERC), and the Fonds de Recherche du Québec—Santé (FRQS). E.L. is a senior scholar of the FRQS. J.C.A.P. was supported by doctoral scholarships from the FRQS, McGill University, and the IRCM.

Availability of data and materials

The data generated and/or analysed during the current study have been deposited in NCBI's Gene Expression Omnibus (Padilla et al., 2023) and are

accessible through GEO Series accession number GSE225471 (https://www.ncbi.nlm.nih.gov/geo/query/acc.cgi?acc=GSE225471).

Declarations

Ethics approval and consent to participate
Not applicable.

Consent for publication
Not applicable.

Competing interests
The authors declare no competing interests.

Received: 21 April 2023 Accepted: 3 August 2023
Published online: 22 September 2023

References

1. Théry C, Witwer KW, Aikawa E, Alcaraz MJ, Anderson JD, Andriantsitohaina R, Antoniou A, Arab T, Archer F, Atkin-Smith GK, et al. Minimal information for studies of extracellular vesicles 2018 (MISEV2018): a position statement of the International Society for Extracellular Vesicles and update of the MISEV2014 guidelines. J Extracell Vesicles. 2018;7(1):1535750.
2. van Niel G, D'Angelo G, Raposo G. Shedding light on the cell biology of extracellular vesicles. Nat Rev Mol Cell Biol. 2018;19(4):213–28.
3. Maacha S, Bhat AA, Jimenez L, Raza A, Haris M, Uddin S, Grivel J-C. Extracellular vesicles-mediated intercellular communication: roles in the tumor microenvironment and anti-cancer drug resistance. Mol Cancer. 2019;18(1):55.
4. O'Brien K, Breyne K, Ughetto S, Laurent LC, Breakefield XO. RNA delivery by extracellular vesicles in mammalian cells and its applications. Nat Rev Mol Cell Biol. 2020;21(10):585–606.
5. Lefebvre FA, Lecuyer E. Small luggage for a long journey: transfer of vesicle-enclosed small RNA in interspecies communication. Front Microbiol. 2017;8:377.
6. Bovaird S, Patel D, Padilla JA, Lécuyer E. Biological functions, regulatory mechanisms, and disease relevance of RNA localization pathways. FEBS Lett. 2018;592(17):2948–72.
7. Skog J, Würdinger T, van Rijn S, Meijer DH, Gainche L, Sena-Esteves M, Curry WT Jr, Carter BS, Krichevsky AM, Breakefield XO. Glioblastoma microvesicles transport RNA and proteins that promote tumour growth and provide diagnostic biomarkers. Nat Cell Biol. 2008;10(12):1470–6.
8. Nolte-'t Hoen EN, Buermans HP, Waasdorp M, Stoorvogel W, Wauben MH. t Hoen PA: Deep sequencing of RNA from immune cell-derived vesicles uncovers the selective incorporation of small non-coding RNA biotypes with potential regulatory functions. Nucleic Acids Res. 2012;40(18):9272–85.
9. Baglio SR, Rooijers K, Koppers-Lalic D, Verweij FJ, Pérez Lanzón M, Zini N, Naaijkens B, Perut F, Niessen HW, Baldini N, et al. Human bone marrow- and adipose-mesenchymal stem cells secrete exosomes enriched in distinctive miRNA and tRNA species. Stem Cell Res Ther. 2015;6(1):127.
10. Lefebvre FA, Benoit Bouvrette LP, Perras L, Blanchet-Cohen A, Garnier D, Rak J, Lecuyer E. Comparative transcriptomic analysis of human and drosophila extracellular vesicles. Sci Rep. 2016;6:27680.
11. Wang L, Jia Q, Xinnong C, Xie Y, Yang Y, Zhang A, Liu R, Zhuo Y, Zhang J. Role of cardiac progenitor cell-derived exosome-mediated microRNA-210 in cardiovascular disease. J Cell Mol Med. 2019;23(11):7124–31.
12. Shen M, Dong C, Ruan X, Yan W, Cao M, Pizzo D, Wu X, Yang L, Liu L, Ren X, et al. Chemotherapy-induced extracellular vesicle mirnas promote breast cancer stemness by targeting ONECUT2. Can Res. 2019;79(14):3608–21.
13. Haderk F, Schulz R, Iskar M, Cid LL, Worst T, Willmund KV, Schulz A, Warnken U, Seiler J, Benner A, et al. Tumor-derived exosomes modulate PD-L1 expression in monocytes. Sci Immunol. 2017;2(13):eaah5509.
14. Zhao S, Mi Y, Guan B, Zheng B, Wei P, Gu Y, Zhang Z, Cai S, Xu Y, Li X, et al. Tumor-derived exosomal miR-934 induces macrophage M2 polarization to promote liver metastasis of colorectal cancer. J Hematol Oncol. 2020;13(1):156.
15. Chen S, Tang Y, Liu Y, Zhang P, Lv L, Zhang X, Jia L, Zhou Y. Exosomes derived from miR-375-overexpressing human adipose mesenchymal stem cells promote bone regeneration. Cell Prolif. 2019;52(5):e12669.
16. Zhou W, Fong MY, Min Y, Somlo G, Liu L, Palomares MR, Yu Y, Chow A, O'Connor ST, Chin AR, et al. Cancer-secreted miR-105 destroys vascular endothelial barriers to promote metastasis. Cancer Cell. 2014;25(4):501–15.
17. Li L, Li C, Wang S, Wang Z, Jiang J, Wang W, Li X, Chen J, Liu K, Li C, et al. Exosomes derived from hypoxic oral squamous cell carcinoma cells deliver miR-21 to normoxic cells to elicit a prometastatic phenotype. Can Res. 2016;76(7):1770–80.
18. Fang JH, Zhang ZJ, Shang LR, Luo YW, Lin YF, Yuan Y, Zhuang SM. Hepatoma cell-secreted exosomal microRNA-103 increases vascular permeability and promotes metastasis by targeting junction proteins. Hepatology. 2018;68(4):1459–75.
19. Au Yeung CL, Co NN, Tsuruga T, Yeung TL, Kwan SY, Leung CS, Li Y, Lu ES, Kwan K, Wong KK, et al. Exosomal transfer of stroma-derived miR21 confers paclitaxel resistance in ovarian cancer cells through targeting APAF1. Nat Commun. 2016;7:11150.
20. Binenbaum Y, Fridman E, Yaari Z, Milman N, Schroeder A, Ben David G, Shlomi T, Gil Z. Transfer of miRNA in macrophage-derived exosomes induces drug resistance in pancreatic adenocarcinoma. Can Res. 2018;78(18):5287–99.
21. Ren J, Ding L, Zhang D, Shi G, Xu Q, Shen S, Wang Y, Wang T, Hou Y. Carcinoma-associated fibroblasts promote the stemness and chemoresistance of colorectal cancer by transferring exosomal lncRNA H19. Theranostics. 2018;8(14):3932–48.
22. Wang E, Aifantis I. RNA Splicing and Cancer. Trends Cancer. 2020;6(8):631–44.
23. Wang XW, Liu CX, Chen LL, Zhang QC. RNA structure probing uncovers RNA structure-dependent biological functions. Nat Chem Biol. 2021;17(7):755–66.
24. Roth MJ, Forbes AJ, Boyne MT 2nd, Kim YB, Robinson DE, Kelleher NL. Precise and parallel characterization of coding polymorphisms, alternative splicing, and modifications in human proteins by mass spectrometry. Mol Cell Proteomics. 2005;4(7):1002–8.
25. Nilsen TW, Graveley BR. Expansion of the eukaryotic proteome by alternative splicing. Nature. 2010;463(7280):457–63.
26. Kim MS, Pinto SM, Getnet D, Nirujogi RS, Manda SS, Chaerkady R, Madugundu AK, Kelkar DS, Isserlin R, Jain S, et al. A draft map of the human proteome. Nature. 2014;509(7502):575–81.
27. Wilkinson ME, Charenton C, Nagai K. RNA Splicing by the Spliceosome. Annu Rev Biochem. 2020;89:359–88.
28. Kuhn CD. RNA versatility governs tRNA function: Why tRNA flexibility is essential beyond the translation cycle. BioEssays. 2016;38(5):465–73.
29. Baßler J, Hurt E. Eukaryotic ribosome assembly. Annu Rev Biochem. 2019;88:281–306.
30. Leppek K, Das R, Barna M. Functional 5′UTR mRNA structures in eukaryotic translation regulation and how to find them. Nat Rev Mol Cell Biol. 2018;19(3):158–74.
31. Quévillon Huberdeau M, Simard MJ. A guide to microRNA-mediated gene silencing. FEBS J. 2019;286(4):642–52.
32. Flores JK, Ataide SF. Structural changes of RNA in complex with proteins in the SRP. Front Mol Biosci. 2018;5:7.
33. Batagov AO, Kurochkin IV. Exosomes secreted by human cells transport largely mRNA fragments that are enriched in the 3′-untranslated regions. Biol Direct. 2013;8:12.
34. Tosar JP, Gámbaro F, Sanguinetti J, Bonilla B, Witwer KW, Cayota A. Assessment of small RNA sorting into different extracellular fractions revealed by high-throughput sequencing of breast cell lines. Nucleic Acids Res. 2015;43(11):5601–16.
35. Chakrabortty SK, Prakash A, Nechooshtan G, Hearn S, Gingeras TR. Extracellular vesicle-mediated transfer of processed and functional RNY5 RNA. RNA (New York, NY). 2015;21(11):1966–79.
36. Chen Q, Yan M, Cao Z, Li X, Zhang Y, Shi J, Feng GH, Peng H, Zhang X, Zhang Y, et al. Sperm tsRNAs contribute to intergenerational inheritance of an acquired metabolic disorder. Science (New York, NY). 2016;351(6271):397–400.
37. Sharma U, Conine CC, Shea JM, Boskovic A, Derr AG, Bing XY, Belleannee C, Kucukural A, Serra RW, Sun F, et al. Biogenesis and function of tRNA

fragments during sperm maturation and fertilization in mammals. Science (New York, NY). 2016;351(6271):391–6.
38. Cambier L, de Couto G, Ibrahim A, Echavez AK, Valle J, Liu W, Kreke M, Smith RR, Marbán L, Marbán E. Y RNA fragment in extracellular vesicles confers cardioprotection via modulation of IL-10 expression and secretion. EMBO Mol Med. 2017;9(3):337–52.
39. Ratajczak J, Miekus K, Kucia M, Zhang J, Reca R, Dvorak P, Ratajczak MZ. Embryonic stem cell-derived microvesicles reprogram hematopoietic progenitors: evidence for horizontal transfer of mRNA and protein delivery. Leukemia. 2006;20(5):847–56.
40. Valadi H, Ekström K, Bossios A, Sjöstrand M, Lee JJ, Lötvall JO. Exosome-mediated transfer of mRNAs and microRNAs is a novel mechanism of genetic exchange between cells. Nat Cell Biol. 2007;9(6):654–9.
41. Zomer A, Maynard C, Verweij FJ, Kamermans A, Schäfer R, Beerling E, Schiffelers RM, de Wit E, Berenguer J, Ellenbroek SIJ, et al. In Vivo imaging reveals extracellular vesicle-mediated phenocopying of metastatic behavior. Cell. 2015;161(5):1046–57.
42. Hinger SA, Cha DJ, Franklin JL, Higginbotham JN, Dou Y, Ping J, Shu L, Prasad N, Levy S, Zhang B, et al. Diverse long RNAs are differentially sorted into extracellular vesicles secreted by colorectal cancer cells. Cell Rep. 2018;25(3):715–725.e714.
43. van Dijk EL, Jaszczyszyn Y, Naquin D, Thermes C. The third revolution in sequencing technology. Trends Genet. 2018;34(9):666–81.
44. Deamer D, Akeson M, Branton D. Three decades of nanopore sequencing. Nat Biotechnol. 2016;34(5):518–24.
45. Wang Y, Zhao Y, Bollas A, Wang Y, Au KF. Nanopore sequencing technology, bioinformatics and applications. Nat Biotechnol. 2021;39(11):1348–65.
46. Grünberger F, Ferreira-Cerca S, Grohmann D. Nanopore sequencing of RNA and cDNA molecules in Escherichia coli. RNA (New York, NY). 2022;28(3):400–17.
47. Gonzalez L, Nebreda AR. RINGO/Speedy proteins, a family of non-canonical activators of CDK1 and CDK2. Semin Cell Dev Biol. 2020;107:21–7.
48. Gleeson J, Leger A, Prawer YDJ, Lane TA, Harrison PJ, Haerty W, Clark MB. Accurate expression quantification from nanopore direct RNA sequencing with NanoCount. Nucleic Acids Res. 2021;50(4):e19–e19.
49. Tang AD, Soulette CM, van Baren MJ, Hart K, Hrabeta-Robinson E, Wu CJ, Brooks AN. Full-length transcript characterization of SF3B1 mutation in chronic lymphocytic leukemia reveals downregulation of retained introns. Nat Commun. 2020;11(1):1438.
50. Andaloussi SE, Mager I, Breakefield XO, Wood MJ. Extracellular vesicles: biology and emerging therapeutic opportunities. Nat Rev Drug Discov. 2013;12(5):347–57.
51. Fafián-Labora JA, O'Loghlen A. Classical and nonclassical intercellular communication in senescence and ageing. Trends Cell Biol. 2020;30(8):628–39.
52. Robbins PD, Morelli AE. Regulation of immune responses by extracellular vesicles. Nat Rev Immunol. 2014;14(3):195–208.
53. Yoon YJ, Kim OY, Gho YS. Extracellular vesicles as emerging intercellular communicasomes. BMB Rep. 2014;47(10):531–9.
54. Yáñez-Mó M, Siljander PRM, Andreu Z, Bedina Zavec A, Borràs FE, Buzas EI, Buzas K, Casal E, Cappello F, Carvalho J, et al. Biological properties of extracellular vesicles and their physiological functions. J Extracell Vesicles. 2015;4(1):27066.
55. Lo Cicero A, Stahl PD, Raposo G. Extracellular vesicles shuffling intercellular messages: for good or for bad. Curr Opin Cell Biol. 2015;35:69–77.
56. Li Y, Zhao J, Yu S, Wang Z, He X, Su Y, Guo T, Sheng H, Chen J, Zheng Q, et al. Extracellular vesicles long RNA sequencing reveals abundant mRNA, circRNA, and lncRNA in human blood as potential biomarkers for cancer diagnosis. Clin Chem. 2019;65(6):798–808.
57. Mori MA, Ludwig RG, Garcia-Martin R, Brandão BB, Kahn CR. Extracellular miRNAs: from biomarkers to mediators of physiology and disease. Cell Metab. 2019;30(4):656–73.
58. Srinivasan S, Treacy R, Herrero T, Olsen R, Leonardo TR, Zhang X, DeHoff P, To C, Poling LG, Fernando A, et al. Discovery and verification of extracellular miRNA biomarkers for non-invasive prediction of pre-eclampsia in asymptomatic women. Cell Rep Med. 2020;1(2):100013.
59. Shan S, Yang Y, Jiang J, Yang B, Yang Y, Sun F, Zhang J, Lin Y, Xu H. Extracellular vesicle-derived long non-coding RNA as circulating biomarkers for endometriosis. Reprod Biomed Online. 2022;44(5):923–33.
60. Puffer RC, Cumba Garcia LM, Himes BT, Jung MY, Meyer FB, Okonkwo DO, Parney IF. Plasma extracellular vesicles as a source of biomarkers in traumatic brain injury. J Neurosurg. 2020;134(6):1921–8.
61. Vader P, Breakefield XO, Wood MJA. Extracellular vesicles: emerging targets for cancer therapy. Trends Mol Med. 2014;20(7):385–93.
62. Quesenberry PJ, Aliotta J, Deregibus MC, Camussi G. Role of extracellular RNA-carrying vesicles in cell differentiation and reprogramming. Stem Cell Res Ther. 2015;6(1):153.
63. Dinger ME, Mercer TR, Mattick JS. RNAs as extracellular signaling molecules. J Mol Endocrinol. 2008;40(4):151–9.
64. Abels ER, Breakefield XO. Introduction to Extracellular Vesicles: Biogenesis, RNA Cargo Selection, Content, Release, and Uptake. Cell Mol Neurobiol. 2016;36(3):301–12.
65. Crescitelli R, Lasser C, Szabo TG, Kittel A, Eldh M, Dianzani I, Buzas EI, Lotvall J. Distinct RNA profiles in subpopulations of extracellular vesicles: apoptotic bodies, microvesicles and exosomes. J Extracell Vesicles. 2013;2:20677.
66. Herrera M, Llorens C, Rodríguez M, Herrera A, Ramos R, Gil B, Candia A, Larriba MJ, Garre P, Earl J, et al. Differential distribution and enrichment of non-coding RNAs in exosomes from normal and Cancer-associated fibroblasts in colorectal cancer. Mol Cancer. 2018;17(1):114.
67. Magaña SM, Peterson TE, Evans JE, Decker PA, Simon V, Eckel-Passow JE, Daniels DJ, Parney IF. Pediatric brain tumor cell lines exhibit miRNA-depleted Y RNA-enriched extracellular vesicles. J Neurooncol. 2022;156(2):269–79.
68. Sousa D, Matthiesen R, Lima RT, Vasconcelos MH. Deep sequencing analysis reveals distinctive non-coding RNAs when comparing tumor multidrug-resistant cells and extracellular vesicles with drug-sensitive counterparts. Cancers (Basel). 2020;12(1):200.
69. van Hoof A, Lennertz P, Parker R. Yeast exosome mutants accumulate 3′-extended polyadenylated forms of U4 small nuclear RNA and small nucleolar RNAs. Mol Cell Biol. 2000;20(2):441–52.
70. Kuai L, Fang F, Butler JS, Sherman F. Polyadenylation of rRNA in Saccharomyces cerevisiae. Proc Natl Acad Sci USA. 2004;101(23):8581–6.
71. Houseley J, Tollervey D. Yeast Trf5p is a nuclear poly(A) polymerase. EMBO Rep. 2006;7(2):205–11.
72. Slomovic S, Laufer D, Geiger D, Schuster G. Polyadenylation of ribosomal RNA in human cells. Nucleic Acids Res. 2006;34(10):2966–75.
73. Aguilar LC, Paul B, Reiter T, Gendron L, Arul NambiRajan A, Montpetit R, Trahan C, Pechmann S, Oeffinger M, Montpetit B. Altered rRNA processing disrupts nuclear RNA homeostasis via competition for the poly(A)-binding protein Nab2. Nucleic Acids Res. 2020;48(20):11675–94.
74. Porter LA, Dellinger RW, Tynan JA, Barnes EA, Kong M, Lenormand JL, Donoghue DJ. Human speedy: a novel cell cycle regulator that enhances proliferation through activation of Cdk2. J Cell Biol. 2002;157(3):357–66.
75. Gastwirt RF, McAndrew CW, Donoghue DJ. Speedy/RINGO regulation of CDKs in cell cycle, checkpoint activation and apoptosis. Cell cycle (Georgetown, Tex). 2007;6(10):1188–93.
76. Cheng A, Solomon MJ. Speedy/Ringo C regulates S and G2 phase progression in human cells. Cell cycle (Georgetown, Tex). 2008;7(19):3037–47.
77. Byrne A, Beaudin AE, Olsen HE, Jain M, Cole C, Palmer T, DuBois RM, Forsberg EC, Akeson M, Vollmers C. Nanopore long-read RNAseq reveals widespread transcriptional variation among the surface receptors of individual B cells. Nat Commun. 2017;8:16027.
78. Hu Y, Fang L, Chen X, Zhong JF, Li M, Wang K. LIQA: long-read isoform quantification and analysis. Genome Biol. 2021;22(1):182.
79. Fabbiano F, Corsi J, Gurrieri E, Trevisan C, Notarangelo M, D'Agostino VG. RNA packaging into extracellular vesicles: an orchestra of RNA-binding proteins? J Extracell Vesicles. 2020;10(2):e12043.
80. Benoit Bouvrette LP, Blanchette M, Lécuyer E. Bioinformatics approaches to gain insights into cis-regulatory motifs involved in mRNA Localization. Adv Exp Med Biol. 2019;1203:165–94.
81. Garcia-Martin R, Wang G, Brandão BB, Zanotto TM, Shah S, Kumar Patel S, Schilling B, Kahn CR. MicroRNA sequence codes for small extracellular vesicle release and cellular retention. Nature. 2022;601(7893):446–51.
82. Begik O, Lucas MC, Pryszcz LP, Ramirez JM, Medina R, Milenkovic I, Cruciani S, Liu H, Vieira HGS, Sas-Chen A, et al. Quantitative profiling of pseudouridylation dynamics in native RNAs with nanopore sequencing. Nat Biotechnol. 2021;39(10):1278–91.
83. Leger A, Amaral PP, Pandolfini L, Capitanchik C, Capraro F, Miano V, Migliori V, Toolan-Kerr P, Sideri T, Enright AJ, et al. RNA modifications

detection by comparative Nanopore direct RNA sequencing. Nat Commun. 2021;12(1):7198.
84. Stephenson W, Razaghi R, Busan S, Weeks KM, Timp W, Smibert P. Direct detection of RNA modifications and structure using single-molecule nanopore sequencing. Cell Genom. 2022;2(2):100097.
85. Lefebvre FA, Cody NAL, Bouvrette LPB, Bergalet J, Wang X, Lecuyer E. CeFra-seq: systematic mapping of RNA subcellular distribution properties through cell fractionation coupled to deep-sequencing. Methods (San Diego, Calif). 2017;126:138–48.
86. Benoit Bouvrette LP, Cody NAL, Bergalet J, Lefebvre FA, Diot C, Wang X, Blanchette M, Lecuyer E. CeFra-seq reveals broad asymmetric mRNA and noncoding RNA distribution profiles in Drosophila and human cells. RNA (New York, NY). 2018;24(1):98–113.
87. Ewels PA, Peltzer A, Fillinger S, Patel H, Alneberg J, Wilm A, Garcia MU, Di Tommaso P, Nahnsen S. The nf-core framework for community-curated bioinformatics pipelines. Nat Biotechnol. 2020;38(3):276–8.
88. De Coster W, D'Hert S, Schultz DT, Cruts M, Van Broeckhoven C. NanoPack: visualizing and processing long-read sequencing data. Bioinformatics (Oxford, England). 2018;34(15):2666–9.
89. Li H. Minimap2: pairwise alignment for nucleotide sequences. Bioinformatics (Oxford, England). 2018;34(18):3094–100.
90. Ramírez F, Ryan DP, Grüning B, Bhardwaj V, Kilpert F, Richter AS, Heyne S, Dündar F, Manke T. deepTools2: a next generation web server for deep-sequencing data analysis. Nucleic Acids Res. 2016;44(W1):W160–5.
91. Liao Y, Smyth GK, Shi W. The R package Rsubread is easier, faster, cheaper and better for alignment and quantification of RNA sequencing reads. Nucleic Acids Res. 2019;47(8):e47–e47.
92. Love MI, Huber W, Anders S. Moderated estimation of fold change and dispersion for RNA-seq data with DESeq2. Genome Biol. 2014;15(12):550.
93. Ge SX, Son EW, Yao R. iDEP: an integrated web application for differential expression and pathway analysis of RNA-Seq data. BMC Bioinformatics. 2018;19(1):534.
94. Raudvere U, Kolberg L, Kuzmin I, Arak T, Adler P, Peterson H, Vilo J. g:Profiler: a web server for functional enrichment analysis and conversions of gene lists (2019 update). Nucleic Acids Res. 2019;47(W1):W191–w198.
95. Egorov AA, Sakharova EA, Anisimova AS, Dmitriev SE, Gladyshev VN, Kulakovskiy IV. svist4get: a simple visualization tool for genomic tracks from sequencing experiments. BMC Bioinformatics. 2019;20(1):113.

Publisher's Note